Design and Implementation of a Photovoltaic Grid-Connected Micro-Inverter with Power Factor Correction Technology

Yu-Kun Chen, Tsorng-Juu Liang, *Senior Member, IEEE*, and Wei-Chia Wu,
Department of Electrical Engineering/Advanced Optoelectronic Technology Center (AOTC)
/Green Energy Electronics Research Center (GREERC)
National Cheng Kung University, Tainan, Taiwan
Email: tjliang@mail.ncku.edu.tw

***Abstract*—In this paper, a photovoltaic (PV) gird-connected micro-inverter controlled by power factor correction (PFC) controller is implemented. The PFC controller is adopted to control the inverter output current sinusoidally. Besides, the maximum power point tracking control circuit can get the maximum power form PV modules. The duality between the PFC circuit and the inverter circuit is presented first. Then, the PFC design rules is applied in the inverter circuit. However, the flyback inverter controlled by boundary conduction mode (BCM) PFC IC will cause a high third harmonic component from the analysis. Hence, the third harmonic injection method is estimated and analyzed to improve the output current total harmonic distortion. Finally, a 300W grid-connected flyback micro-inverter with BCM control based on L6561 PFC controller is implemented to verify the feasibility. Input voltage is 20V to 40V and the peak power is 300 W from PV simulator, and the output voltage is 220Vac/60Hz. The highest efficiency of the micro-inverter is 92.8%.**

***Index Terms*—Power factor correction, Duality, Grid-connected micro-inverter.**

Ⅰ. INTRODUCTIONS

Due to the global warming, researches for implementing renewable energy such as solar energy, wind energy, ocean energy, biofuel energy, geothermal energy, and etc become highly attractive [1]. Solar energy is clean, easily-accessible and inexhaustible energy. Solar power system can be classified into three types: stand-alone photovoltaic (PV) system, hybrid PV system and grid-connected PV system [2]-[4]. Stand-alone PV system provides electricity to the certain load from PV modules directly without connecting to the grid. It is suitable to be applied in remote isolated regions, islands, or other emergency occasions. However, it has to be equipped with rechargeable batteries for stable power conditioning in stand-alone PV system.

Hybrid PV system are commonly combined with wind turbines or diesel generators. If it is on-grid, hybrid PV system will act like grid-connected PV system that PV and grid provide electricity to the load and charge batteries as well. If it is off-grid, hybrid PV system will act like stand-alone PV system that all energy sources (including batteries) supply electricity stably.

Grid-connected PV system is connected directly to the electrical grid. If the PV system cannot provide enough electricity to the load, the grid will supply electricity to meet the demand. Grid-connected PV system requires no batteries to store energy because of the fact that the redundant energy will be imported to the grid.

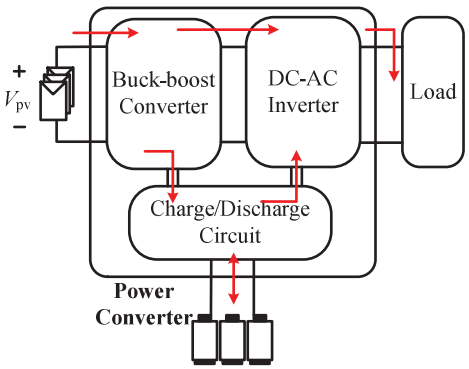

Fig.1 Stand-alone photovoltaic (PV) system

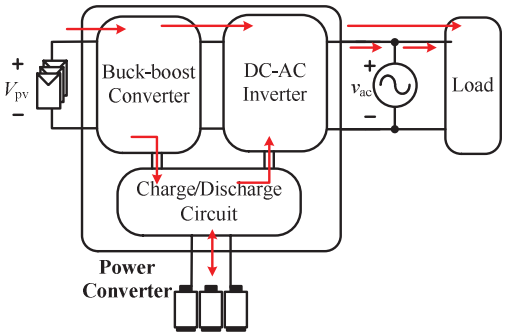

Fig.2 Hybrid PV system

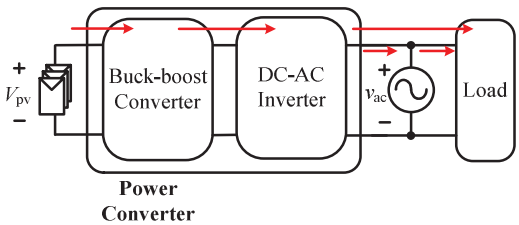

Fig.3 Grid-connected PV system

Since PV modules are connected in series, even one module shaded by nearby buildings, or covered with leaves and dust will reduce output power. In other words, when one module in a series is shaded, the output of series-connected PV modules reacts like all modules are shaded, and it is called “shading effect” [5]-[9].

Therefore, distributed PV systems are developed to overcome the shading effect [10]-[11]. The distributed PV system which is also called AC modules composed of a PV module and a micro-inverter, and output is connected to the grid, as shown in Fig.4

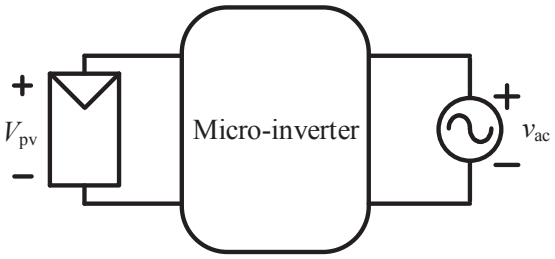

Fig.4 AC module

Ⅱ、DUALITY BETWEEN PFC AND INVERTER

The PFC system and the grid-connected inverter both control the grid current. The PFC system controls the input current track grid voltage sinusoidally. On the other hand, the inverter output current has be sinusoidal and in phase with the grid voltage. In addition, AC to DC converters are controlled to reduce the input current total harmonic distortion (THD_i) by PFC. The inverter also needs low output current distortion. Therefore, these two controllers can be implemented by the same design rule.

The circuit characteristics of flyback topology operated at BCM control are analyzed. The duality between the PFC and the inverter and analysis of the AC components are also illustrated in following section.

a. Flyback converter with PFC circuit

The typical system diagram of flyback converter with PFC is shown in Fig. 5, and Fig. 6 shows the key waveforms of flyback converter operates under BCM.

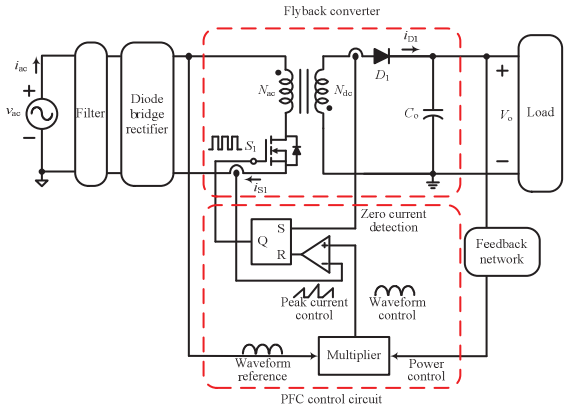

Fig.5 Flyback converter with PFC circuit

According to the volt-second balance law, the equations of switch turn-on time, turn-off time and period are:

$$t_{ON}(\theta) \equiv \frac{L_p \cdot I_{S1,pk} \cdot \sin(\theta)}{V_{ac,pk} \cdot \sin(\theta)} = \frac{L_p \cdot I_{S1,pk}}{V_{ac,pk}} \tag{1}$$

$$t_{OFF}(\theta) \equiv \frac{L_s \cdot I_{D1,pk} \cdot \sin(\theta)}{V_{dc}} = \frac{\frac{L_p}{n^2} \cdot n \cdot I_{S1,pk} \cdot \sin(\theta)}{V_{dc}} = \frac{L_p \cdot I_{S1,pk} \cdot \sin(\theta)}{n \cdot V_{dc}} \tag{2}$$

$$T(\theta) \equiv t_{ON}(\theta) + t_{OFF}(\theta) = (L_p \cdot I_{S1,pk}) \cdot \frac{n \cdot V_{dc} + V_{ac,pk} \cdot \sin(\theta)}{n \cdot V_{dc} \cdot V_{ac,pk}} \tag{3}$$

According to Fig.5, the average current of the switch S_1 is equal to the AC side current, and the equation of AC side current is:

$$\begin{aligned} i_{ac,avg}(\theta) = i_{S1,avg}(\theta) &= \frac{1}{2} I_{S1,pk} \cdot \sin(\theta) \cdot \frac{t_{ON}(\theta)}{T(\theta)} \\ &= \frac{1}{2} \frac{I_{S1,pk} \cdot \sin(\theta)}{1 + \frac{V_{ac,pk} \cdot \sin(\theta)}{n \cdot V_{dc}}} \end{aligned} \tag{4}$$

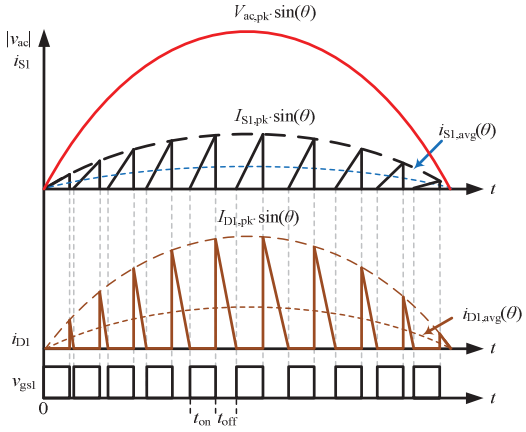

Fig.6 The key waveforms of flyback converter with BCM PWM control

b. Flyback inverter with grid-connected circuit

The typical system diagram of flyback inverter with grid-connected is shown in Fig. 7, and Fig. 8 shows the key waveforms of flyback inverter operates under BCM.

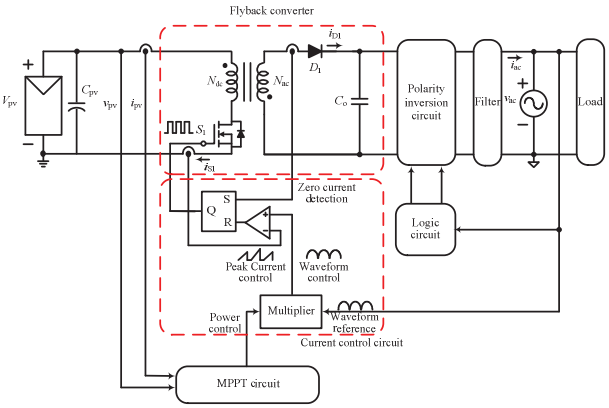

Fig.7 Flyback inverter with grid-connected circuit

According to the volt-second balance law, the equations of switch turn-on time, turn-off time and period are:

$$t_{ON}(\theta) \equiv \frac{L_p \cdot I_{S1,pk} \cdot \sin(\theta)}{V_{dc}} = \frac{\frac{L_s}{n^2} \cdot n \cdot I_{D1,pk} \cdot \sin(\theta)}{V_{dc}} = \frac{L_s \cdot I_{D1,pk} \cdot \sin(\theta)}{n \cdot V_{dc}} \tag{5}$$

$$t_{OFF}(\theta) \equiv \frac{L_s \cdot I_{D1,pk} \cdot \sin(\theta)}{V_{ac,pk} \cdot \sin(\theta)} = \frac{L_s \cdot I_{D1,pk}}{V_{ac,pk}} \tag{6}$$

$$T(\theta) \equiv t_{ON}(\theta) + t_{OFF}(\theta) = (L_s \cdot I_{D1,pk}) \cdot \frac{n \cdot V_{dc} + V_{ac,pk} \cdot \sin(\theta)}{n \cdot V_{dc} \cdot V_{ac,pk}} \tag{7}$$

According to Fig. 7, the average current of the switch S_1 is reflected to the AC side through flyback transformer, and the average AC side current in one switching period is shown in equation (8):

$$i_{ac,avg}(\theta) = i_{D1,avg}(\theta) = \frac{1}{2} I_{D1,pk} \cdot \sin(\theta) \cdot \frac{t_{OFF}(\theta)}{T(\theta)} = \frac{1}{2} \frac{I_{D1,pk} \cdot \sin(\theta)}{1 + \frac{V_{ac,pk} \cdot \sin(\theta)}{n \cdot V_{dc}}} \quad (8)$$

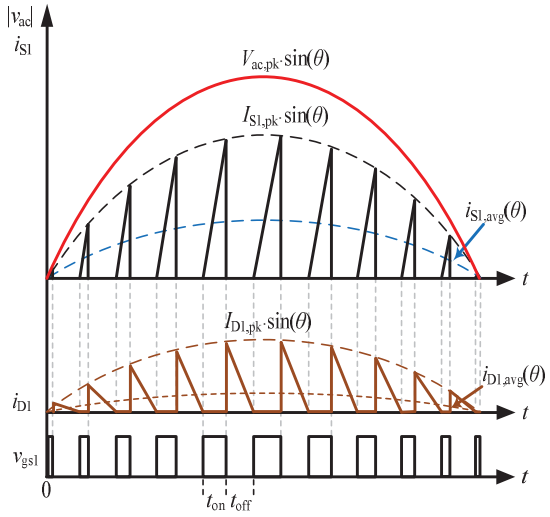

Fig.8 The key waveforms of flyback inverter with BCM PWM control

From equation (4) and (8), the average of the AC current ($i_{ac,avg}$) and AC components are the same when the PFC circuit and the inverter are operated under the same power rating, the same operating frequency, and the same duty ratio. Furthermore, the same power rating means that the switch peak current of PFC S_1 ($i_{S1,pk}$) is equal to the diode peak current of inverter ($i_{D1,pk}$). The same operating frequency means that the equation (3) is equal to (7). The same duty ration means that the ac side of PFC turn-on time ($t_{ON}(\theta)$) is equal to the ac side of inverter turn-off time ($t_{OFF}(\theta)$).

By using SIMPLIS® circuit simulation software to simulate the operation condition on the same power, frequency, and duty cycle, the correspondent spectrums can be received by Fourier analysis of both AC currents $i_{ac,avg}$. In Fig. 9 and Fig. 10, we could found both the high frequency response and low frequency response have the same spectrum. The main reason that affects the high frequency spectrum is that the magnetizing inductor of transformer and operation frequency of converter is also affected by it. On the other hand, the main cause that affects the low frequency spectrum is average current, and average current is determined by the design of turn ratio.

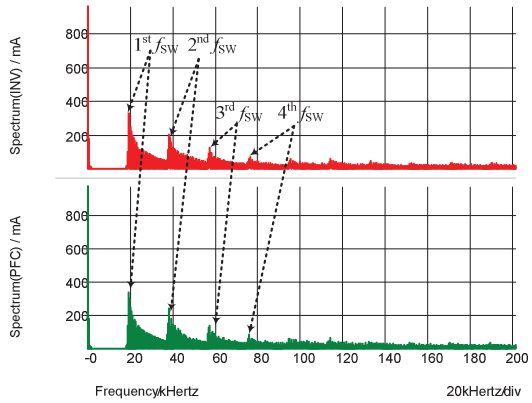

Fig.9 Fourier analysis for high frequency AC currents of inverter circuit and PFC circuit.

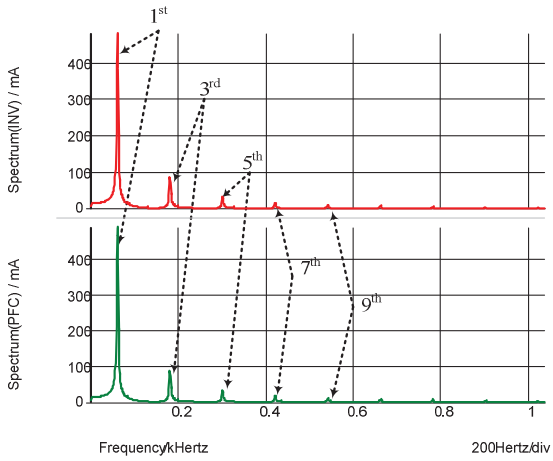

Fig.10 Fourier analysis for low frequency AC currents of inverter circuit and PFC circuit.

Accordingly, this thesis controls an inverter by PFC IC because of the fact that the duality between PFC and inverter. Table 3.1 shows the comparisons between flyback PFC and flyback inverter.

Table 3.1 Comparisons between flyback PFC and flyback inverter.

Compare point	Flyback converter with power factor corrected circuit	Flyback inverter with grid-connected circuit
Power flow direction	AC to DC	DC to AC
AC side current	Average current of switch	Average current of diode
AC to DC/ DC to AC	By diode bridge rectifier	By phase detector to inverse polarity and control switch
Control power signal	Feedback output voltage signal	Feedback input MPPT signal

Ⅲ、CIRCUIT PARAMETER DESIGN

This paper presents a grid-connected flyback-inverter controlled by PFC controller L6561 [12]-[20]. The circuit parameter design are focused on two parts: (a) PFC controller settings (including an additional increase of the circuit, in order to achieve grid-connected inverter functional), (b) circuit parameter design of inverter.

The specification of the flyback inverter is shown in the table 2.

A. PFC controller settings

The flyback inverter, as shown in Fig.11, performs energy flow from the dc to the ac side, by using two identical secondary windings.

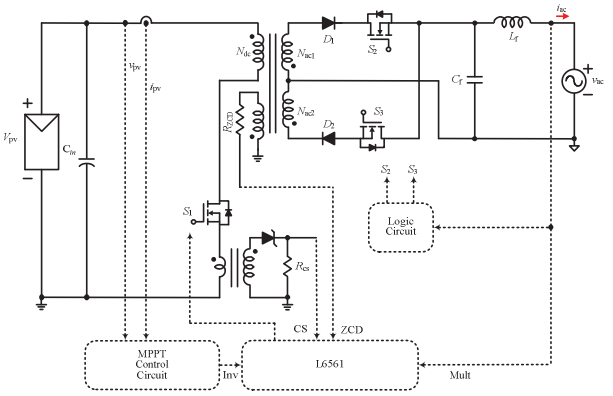

Fig.11 Flyback inverter topology diagram with L6561

The pin5 of L6561 is use to detect the demagnetizing, when magnetizing current of the transformer is decreased to zero; the use of a transformer in series with the switch as a control signal to detect the inductor currents to the pin4 of L6561 (CS); After utility power sine wave rectifier as a reference to the pin3 of L6561 (Mult); using the maximum power controller as a power control signal system to the pin1 of L6561 (Inv).

B. Circuit parameter design of inverter

The following application of the design process for the reverse flyback PFC circuit design process. Flyback converter using the conversion ratio formula can be obtained transformer turns ratio n, as in formula (9).

$$n=\frac{N_{ac}}{N_{dc}}=\frac{D\cdot V_{ac,pk}}{(1-D)\cdot V_{dc}} \tag{9}$$

From equation (1), (2), the minimum conduction time occurred at the peak grid voltage and the duty ratio can be derived as equation (10).

$$D_{\min}=\frac{t_{ON}(\frac{\pi}{2})}{t_{ON}(\frac{\pi}{2})+t_{OFF}(\frac{\pi}{2})}=\frac{V_{dc}}{V_{dc}+V_{ac,pk}/n} \tag{10}$$

When the mains voltage is positive half cycle and the switch S_1 is turned off, the AC side of the diode D_1 and the voltage across the switch S_2 is at least twice the peak grid voltage, as shown in equation (11). S_1 which is subject to the maximum current $I_{ds1,pk}$ which shown in equation (12). Average current diode D_1 is shown in equation (13). At negative half-cycle the circuit condition is symmetrical to the positive half-cycle.

$$V_{ds2}=V_{D1}=2\cdot V_{ac,pk} \tag{11}$$

$$I_{ds1,pk}=I_{D1,pk}=\frac{2\cdot\pi\cdot I_{dc}}{n\cdot[\int_0^{\pi}[\sin(\theta)+k\sin(3\theta)]\cdot(\frac{\frac{\sin(\theta)}{V_{dc}/n}}{\frac{1}{V_{ac,pk}}+\frac{\sin(\theta)}{V_{dc}/n}})d\theta]} \tag{12}$$

$$I_{D1,avg}=\frac{1}{2}\int_0^{\pi}\frac{I_{D1,pk}\cdot[\sin(\theta)+k\sin(3\theta)]}{1+\frac{v_{ac,pk}\cdot\sin(\theta)}{n\cdot v_{dc}}}d\theta \tag{13}$$

Due to BCM operation, the AC side magnetizing inductance is set by the minimum frequency f_{min} as described in equation (14).

$$L_s=\frac{1}{f_{\min}\cdot I_{D1,pk}\cdot(\frac{1}{V_{ac,pk}}+\frac{1}{n\cdot v_{dc}})} \tag{14}$$

The voltage across switch S_1 can be derived in equation (15). And the peak current of S_1 is shown in equation (16).

$$V_{ds1}=V_{dc}+\frac{V_{ac,pk}}{n} \tag{15}$$

$$I_{S1,pk}=n\cdot I_{D1,pk} \tag{16}$$

Ⅳ、ANALYSIS AND DESIGN THIRD HARMONIC INJECTION CIRCUIT

According to equation (8), greater transformer turn ratio n leads the AC side current more close to ideal sinusoidal wave. Conversely, smaller n values causes serious current harmonics, especially 3rd harmonic. The waveforms are shown in Fig. 12.

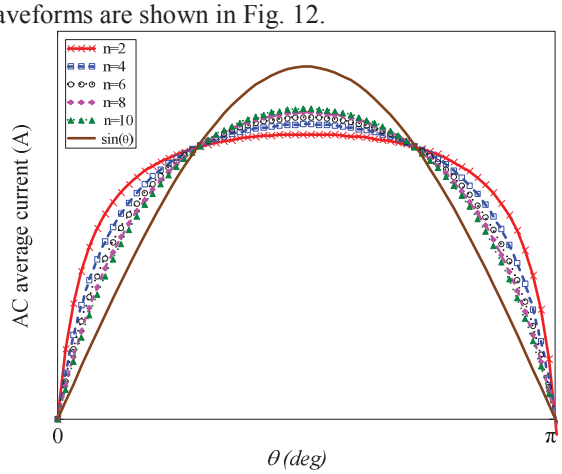

Fig.12 The average AC current with flyback inverter under different transformer turn ratio

To improve this distortion, this paper propose injecting the 3rd harmonic into peak current ($I_{S1,pk}\sin(\theta)$) to reduce the THD. Since the 3rd harmonic is injected, the equation (5) and (6) are rewrote, wherein k is the coefficient of the third harmonic.

$$t_{ON}(\theta)=\frac{L_s\cdot I_{D1,pk}\cdot[\sin(\theta)+k\sin(3\theta)]}{n\cdot V_{dc}} \tag{17}$$

$$t_{OFF}(\theta)=\frac{L_s\cdot I_{D1,pk}\cdot[\sin(\theta)+k\sin(3\theta)]}{V_{ac,pk}\cdot\sin(\theta)} \quad (18)$$

According to the equation (8), (17) and (18), the average AC current with injected the 3rd harmonic is defined by equation (19), and the THD is calculated in equation (20), wherein A_1 is the constituents of fundamental frequency of effective value.

$$i_{ac,avg}(\theta)=\frac{1}{2}\frac{I_{D1,pk}\cdot[\sin(\theta)+k\sin(3\theta)]}{1+\dfrac{V_{ac,pk}\cdot\sin(\theta)}{n\cdot V_{dc}}} \quad (19)$$

$$THD(k)=\frac{\sqrt{[I_{rms}(k)]^2-[A_1(k)]^2}}{I_{rms}(k)} \quad (20)$$

Fig. 13 shows the variation of THD with different injected 3rd harmonic component k and turn ratio n.

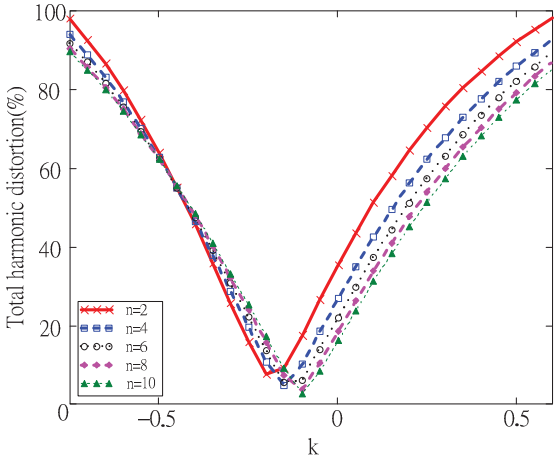

Fig.13 The variation of THD with different injected 3rd harmonic component k and turn ratio n

Fig.14 shows the 3rd harmonic generation circuit, which generates a square wave with the line frequency, and uses a band-pass filter to obtain the 3rd harmonic, after that, adds the fundamental frequency as a reference waveform. Therefore, it can improve THD of the system.

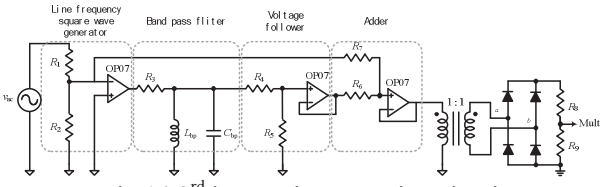

Fig.14 3rd harmonic generation circuit

V、Experimental and simulation results

In this paper, two 150W modules are connected in parallel to achieve the rated power of 300W. Fig. 15 shows the two flyback inverters in parallel of the grid-connected micro-inverter system. Each flyback inverter input is a single PV module. Therefore, its input voltage and input current are applied to the maximum power point tracker. This control signal can be a reference of the flyback inverter. There are two types of the low frequency inverter, full-bridge inverter circuit and center-tapped inverter circuit. Because of the risk of short circuit by using full bridge, both flyback inverters are the low frequency commutation using center-tapped by secondary side. The control signal of polarity judgments and sinusoidal reference voltage of PFC controllers are also provided by the same rectifier circuit. Both flyback inverters share the output of the filter.

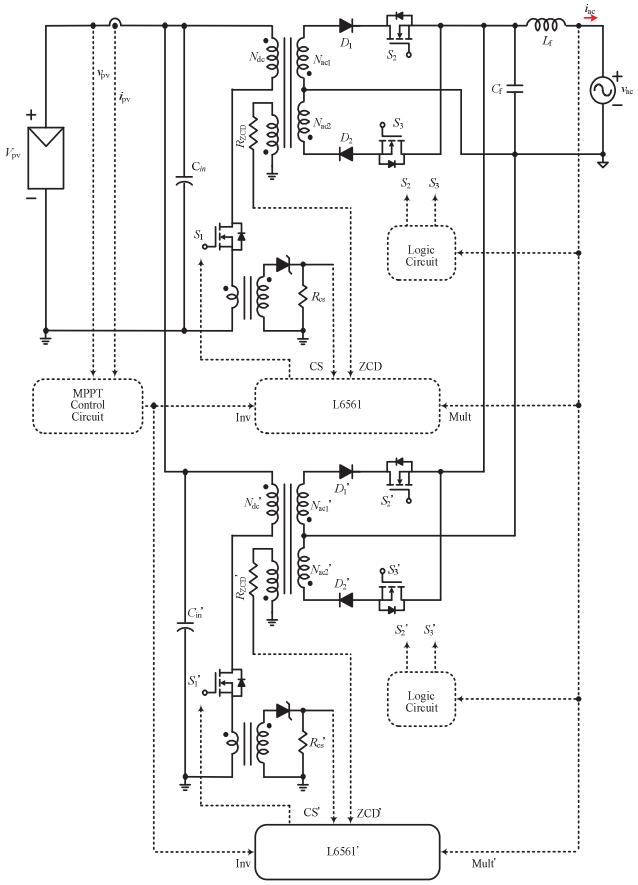

Fig.15 Two flyback micro-inverters in parallel of the grid-connected system

In this paper, a 300W grid-connected flyback micro-inverter with BCM control based on L6561 PFC controller is implemented to verify the feasibility. The 3rd harmonic injection method is adopted by simulation software to improve the output current THD. The related specification of the system and the components used in the system are shown in Table. 2 and Table. 3 respectively.

Table. 2 System specifications

PV panel maximum output power	300 W
DC input voltage	20~40 Vdc
AC output voltage	220 Vac

Table. 3 Component specifications

Transformer design	
L_m	49.8 μH
L_{k1}	0.97 μH
Primary	24 turns
Secondary	96 turns
Circuit design	
S_1	IXTQ96N20P (200 V / 96 A)
S_2 and S_3	IXFR15N80Q (800 V / 13 A)
D_1 and D_2	D05S120 (1200 V / 5 A)
DC input capacitor C_{in}	4700 μF×3
Current transformer turn ratio n_{cs}	1:100
AC filter capacitor C_f	1 μF
AC filter inductor L_f	10 mH

Fig.16 shows the key waveforms of the inverter at full load (150 W). Fig.17 shows the key waveforms of two inverters in parallel at full load (300 W). According to Fig. 16 and Fig. 17, the output current is ringing when V_{gs2} and V_{gs3} are overlapped. Furthermore, the ringing frequency is the same as the resonant frequency which is caused by output filter inductor and capacitor. If the overlapped time is too long, the ringing effect will cause serious output current distortion. Conversely, the short overlapped time can reduce the ringing effect. However, the overlapped time is required or it will cause open circuit and increase the voltage stress on secondary switch and diode.

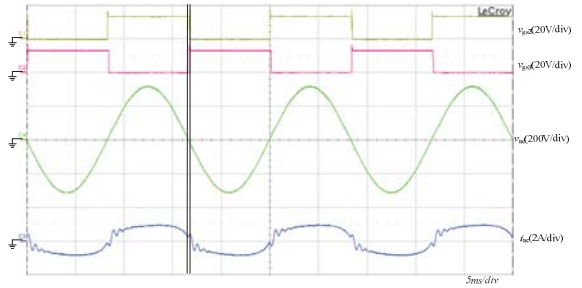

Fig.16 v_{ac} and i_{ac} of the inverter at full load (150 W).

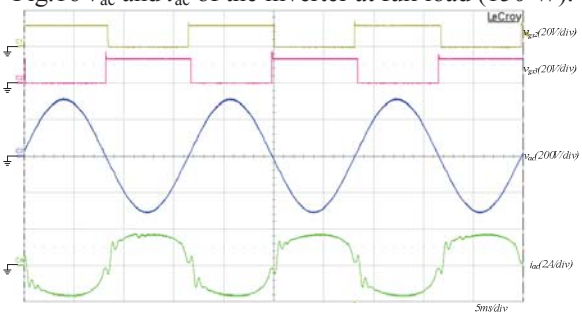

Fig.17 v_{ac} and i_{ac} of two inverters in parallel at full load (300 W).

In order to improve the output current THD, the 3rd harmonic injection method is needed. Fig. 18 shows the simulation results of v_{ac}, i_{ac}, and mult without the 3rd harmonic injection. Fig. 19 shows the simulation results of v_{ac}, i_{ac}, and mult with the 3rd harmonic injection. In addition, comparison between the harmonic spectrum from i_{ac} in Fig.18 and Fig.19 and IEEE Std 1547 [21] is shown in Fig. 20. From the result, the 3rd harmonic injection method can improve the THD and conform to the standard.

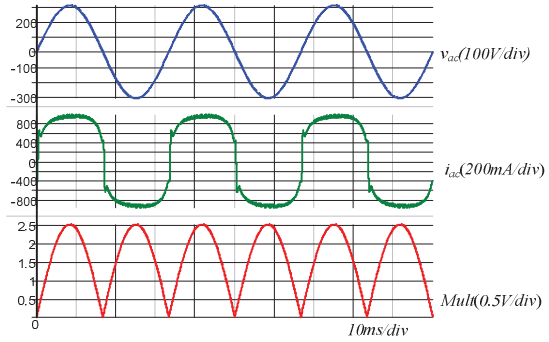

Fig.18 v_{ac}, i_{ac} and mult without the 3rd harmonic injection.

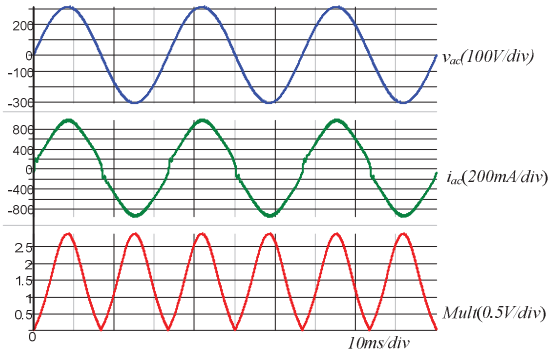

Fig.19 v_{ac}, i_{ac}, and mult with the 3rd harmonic injection.

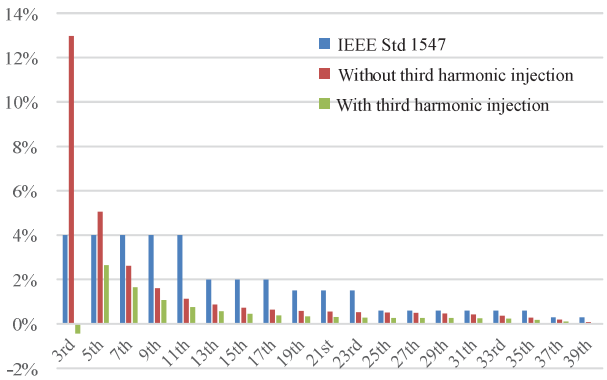

Fig.20 Harmonic spectrum of i_{ac} and IEEE Std 1547.

Fig. 21 shows experiment efficiency curves when input voltage is 30 V and 40 V and output voltage is 220 V_{ac}. The highest efficiency is 92.8% when input voltage is 40 V and output power is 90 W. According to the IEC efficiency standard for PV system, the IEC conversion efficiency is 91.6% when the input voltage is 30 V. According to the CEC efficiency standard, the CEC

conversion efficiency is 91.77% when input voltage is 30 V.

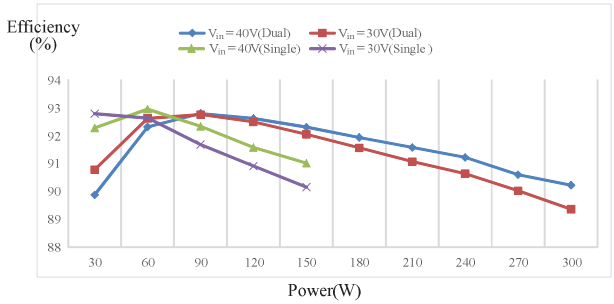

Fig.21 Efficiency curves

VI、CONCLUSIONS

A photovoltaic gird-connected micro-inverter controlled by PFC controller is proposed. The duality between PFC and inverter are proved by simulation. Flyback topology is selected because of simple structure and few components, and is free from energy returning to source. Besides, the center-tapped transformer is used in the flyback micro-inverter to avoid the short circuit damage. Accordingly, the design procedure of flyback PFC can be applied in flyback micro-inverter. The output current of flyback micro-inverter is controlled by the PFC controller which controls output current sinusoidally and the MPPT control is also integrated. The third harmonic injection method is proposed to reduce the output current harmonics, and validated by simulation. Finally, a 300W grid-tied flyback micro-inverter with boundary conduction mode control based on L6561 PFC controller is implemented to verify the feasibility of the proposed theory. Input voltage is 20V to 40V and the peak power is 300 W from PV simulator, and the output voltage is 220Vac/60Hz.

ACKNOWLEDGEMENT

The authors gratefully acknowledge financial support from the Ministry of Science and Technology, Taiwan under project No. 103-2221-E-006-105-MY3

References

[1] Http://www.taipower. com.tw/UpFile/File/CSR/2013.pdf.

[2] M. Kolhe, "Techno-Economic Optimum Sizing of a Stand-Alone Solar Photovoltaic System," IEEE Transactions on, Energy Conversion, vol.24, no.2, pp. 511-519, June 2009.

[3] S. B. Silva, M. A. G. Oliveira, and M. M. Severino, "Sizing and Optimization of Hybrid Photovoltaic, Fuel Cell and Battery System," IEEE (Revista IEEE America Latina), Latin America Transactions, vol.9, no.1, pp. 817-822, March 2011

[4] T. F. Wu, C. H. Chang, L. C. Lin, and C. L. Kuo, "Power Loss Comparison of Single- and Two-Stage Grid-Connected Photovoltaic Systems," IEEE Transactions on , Energy Conversion, vol.26, no.2, pp. 707-715, June 2011

[5] E. Paraskevadaki, S. Papathanassiou, and G. Vokas, "Effects of Partial Shading on the PV Module Characteristic Curves," Materials Science Forum: Applied Electromagnetic Engineering, vol. 670, pp. 391-398, Dec. 2010.

[6] Y. Ueda, T. Oozeki, K. Kurokawa, T. Itou, K. Kitamura, Y. Miyamoto, M. Yokota, and H. Sugihara, "Advanced Analysis of Shading Effect Using Minutely Based Measured Data for PV Systems," International Photovoltaic Science & Engineering Conference, pp. 444-445, 2005.

[7] Y. J. Wang and P. C. Hsu, "Analytical modelling of partial shading and different orientation of photovoltaic modules," IET Trans. Renewable Power Generation, vol. 4, no. 3, pp. 272-282, May 2010.

[8] L. Gao, R. A. Dougal, S. Liu, and A. P. Iotova , "Parallel-Connected Solar PV System to Address Partial and Rapidly Fluctuating Shadow Conditions," IEEE Transactions on, Industrial Applications, vol. 56, no. 5, pp. 1548-1556, Apr. 2009.

[9] S. K. Firth, K. J. Lomas, and S. J. Rees, "A simple model of PV system performance and its use in fault detection," Solar Energy, vol. 84, no. 4, pp. 624-635, Feb. 2010.

[10] Q. Zhang, X. Sun, Y. Zhong, and M. Matsui, "A Novel Topology for Solving the Partial Shading Problem in Photovoltaic Power Generation System," in Proc. IEEE IPEMC, pp. 2130-2135, May 2009.

[11] R. Ramaprabha, B. Mathur, M. Murthy, and S. Madhumitha, "New Configuration of Solar Photo Voltaic Array to Address Partial Shaded Conditions," in Proc. IEEE ICETET, pp. 328-333, Nov. 2010.

[12] A. Ch. Kyritsis, E. C. Tatakis, and N. P. Papanikolaou, "Optimum Design of the Current-Source Flyback Inverter for Decentralized Grid-Connected Photovoltaic Systems," *IEEE Transactions on, Energy Conversion,* vol.23, no.1, pp. 281-293, March. 2008

[13] A. C. Nanakos, E. C. Tatakis, G. S. Dimitrakakis, N. P. Papanikolaou, and A. Ch. Kyritsis, "A Novel Design Methodology Maximizing the Weighted-Efficiency of Flyback Inverter for AC Photovoltaic Modules," *Power Electronics and Applications (EPE 2011),* pp. 1-10, Aug./Sept. 2011

[14] Y. Li and R. Oruganti, "A Flyback-CCM Inverter Scheme for Photovoltaic AC Module Application," *Power Engineering Conference*, pp. 1-6, Dec. 2008

[15] Y. Li and R. Oruganti, "A Low Cost Flyback CCM Inverter for AC Module Application," *IEEE Transactions on, Power Electronics,* vol.27, no.3, pp. 1295-1303, March. 2012

[16] A. Ch. Kyritsis, N. P. Papanikolaou, E. C. Tatakis, and J. C. Kobougias, "Design and Control of a Current Source Flyback Inverter for Decentralized Grid-Connected Photovoltaic Systems," Electronics and Applications, pp. 1-10, Dec. 2005

[17] T. Shimizu, K. Wada, and N. Nakamura, "Flyback-Type Single-Phase Utility Interactive Inverter With Power Pulsation Decoupling on the DC Input for an AC Photovoltaic Module System," IEEE Transactions on, Power Electronics, vol.21, no.5, pp. 1264-1272, Sept. 2006

[18] T. Shimizu, K. Wada, and N. Nakamura, "A Flyback-Type Single Phase Utility Interactive Inverter with Low-Frequency Ripple Current Reduction on the DC Input for an AC Photovoltaic Module System," Power Electronics Specialists Conference, vol.3, pp. 1483-1488, June 2002

[19] A. C. Nanakos, E. C. Tatakis, and N. P. Papanikolaou, "A Weighted-Efficiency-Oriented Design Methodology of Flyback Inverter for AC Photovoltaic Modules," IEEE Transactions on, Power Electronics, vol.27, no.7, pp. 3221-3233, July 2012

[20] STMicroelectronics L6561 datasheet.

[21] IEEE Std1547-2003 – IEEE Standard for Interconnecting Distributed Resources with Electric Power Systems, July 2003.